Theoretical Study of the Electronic Structure of PbS Nanoclusters

R. S. Kane,† R. E. Cohen,† and R. Silbey*,‡

Departments of Chemical Engineering and Department of Chemistry, Massachusetts Institute of Technology, Cambridge, Massachusetts 02139

Received: September 25, 1995; In Final Form: December 5, 1995[⊗]

The semiempirical tight-binding method was used to study the electronic structure of spherical PbS nanocrystals. The effects of spin−orbit coupling were included, and the calculated band gaps were found to agree well with previously published experimental values for PbS clusters. The size dependence of the band gaps was studied for clusters containing as many as 912 atoms (35-Å diameter). Direct diagonalization was used for small clusters, and Lanczos recursion was used to determine the band gaps and the eigenfunctions for the larger clusters. Analysis of the eigenfunctions revealed that the HOMO and LUMO states were spread throughout the cluster. Densities of states for the PbS nanoclusters converged to the bulk density of states, and the joint densities of states were computed as an approximation to the absorption spectra of the nanoclusters.

1. Introduction

Semiconductor nanoclusters,[1] i.e., particles with diameters between 1 and 10 nm, have been the focus of numerous investigations in the past few years. On the experimental side, many research groups have been trying to synthesize nanoclusters of well-defined sizes and have been investigating their electronic and optical properties. A number of theoretical studies[2−6] of the electronic structure of the nanoclusters have also been carried out in order to learn how the bulk properties emerge as the size of the crystallite increases.

It has been observed experimentally that the band gap for semiconductor nanoclusters is larger than the bulk crystal band gap and increases with decreasing cluster size. Since the theoretical methods used for the bulk crystals are not generally valid for the nanocrystallites, which lack the translational symmetry characteristic of an infinite crystal, the theoretical study of the electronic structure of nanocrystallites constitutes a relatively new and challenging area of research. The long-term goal of such studies is to guide experimentalists in their efforts to design novel materials.

The first attempts at explaining the observed blue shift of the absorption spectrum of a semiconductor cluster utilized the particle in a sphere and effective-mass models.[7,8] In the effective-mass approximation, the highest valence band and the lowest conduction band are assumed to have the parabolic form $\hbar^2k^2/(2m^*)$ around their extrema, where m^* is the corresponding effective mass. The effective mass associated with a band is inversely proportional to the curvature of the energy band at its extremum. The finite size of the cluster requires that only certain k values inversely proportional to the radius of the nanocrystal are allowed. This provides the simplest explanation of the quantum size effect on the band gap.

A full wave-mechanical treatment of the problem was reported by Brus.[9] He retained the effective-mass approximation for the kinetic energy of the electron-hole pair. The potential energy term is due to dielectric solvation by atomic core electrons. Brus obtained the following expression for the energy E (defined to be the difference between the band gap of the nanocrystal and the bulk band gap) by taking the solution for the first excited state for a particle in a sphere and assuming that the electron and the hole are uncorrelated:

$$E = \frac{\hbar^2\pi^2}{2R^2}\left[\frac{1}{m_e} + \frac{1}{m_h}\right] - \frac{1.8e^2}{\epsilon_2 R} + \text{polarization term} \quad (1\text{-}1.1)$$

In this case, $k = \pi/R$, where R is the radius of the nanocrystallite. This effective-mass approximation breaks down for large k (i.e., for small R), since the assumption that the energy surfaces are parabolic in k is valid only for small k.

A few other theoretical methods have been introduced. Wang et al.[10] found that the electron-hole-in-a-box model with the effective-mass approximation overestimated the band gap for small PbS clusters. They included the effects of band nonparabolicity and calculated the band gaps for PbS crystallites using a two-band model, with a basis set consisting of sp^3 pseudofunctions centered on the Pb and S atoms.

Lippens and Lannoo[2,3] have used the semiempirical tight-binding method to study the size dependence of the band gap for CdS, ZnS, and CdSe crystallites. The authors used a 13 parameter sp^3s^* model, without the spin−orbit interaction. The crystals studied had a symmetric shape, and dangling orbitals were neglected. The semiempirical Hamiltonian matrix elements were obtained by fitting the bulk band structure, following the approach of Vogl et al.[11] These authors also concluded that the calculations based on the effective-mass approximation strongly overestimate the band gap for crystallites with the smallest sizes.[2] Tight-binding calculations of the band gap for CdSe crystallites with radii between 15 and 20 Å were found to agree well with experiments.[3] The tight-binding method was also successfully used by Ren and Dow[19] to study the electronic structures of surface-hydrogenated Si clusters. The authors used group theory to simplify the diagonalization of their matrices. These and other studies[5,6,10] demonstrate that the tight-binding method gives useful information about semiconductor nanocrystals.

Lead sulfide nanocrystals are the focus of this work. Lead sulfide, because of its small effective mass, shows a large blue-shift in its absorption edge with a small change in cluster size. Bulk lead sulfide has an infrared band gap (0.41 eV)[10] that shifts to the visible region for the nanoclusters. As a result, lead sulfide nanoclusters may be useful in electroluminescent devices such as light-emitting diodes. In addition, lead sulfide nanoclusters are expected to have exceptional third-order nonlinear optical properties[12] and may also be useful in optical devices

† Department of Chemical Engineering.
‡ Department of Chemistry.
[⊗] Abstract published in *Advance ACS Abstracts,* April 1, 1996.

S0022-3654(95)02869-3 CCC: $12.00

such as optical switches. The semiempirical tight-binding method has been used here to study the electronic structure of lead sulfide nanocrystals.

Lead sulfide has the rock salt crystal structure. Its band structure is complicated by large relativistic splittings. To apply the semiempirical tight-binding theory to lead sulfide nanocrystals, Hamiltonian matrix elements first need to be obtained by fitting the bulk band structure. This has already been done by Lent et al.,[13] who used the semiempirical tight-binding method to fit the orthogonalized plane wave band structures of GeTe, SnTe, PbTe, PbSe, and PbS. Their Hamiltonian H, which includes the spin−orbit interaction H_{so}, has the form (for one electron)

$$H = \frac{p^2}{2m} + V + H_{so} + \frac{\hbar^2\nabla^2 V}{8m^2c^2} - \frac{p^4}{8m^3c^2} \qquad (1\text{-}1)$$

where V is the crystal potential and H_{so} is given by

$$H_{so} = \hbar\vec{\sigma}\cdot\frac{(\nabla V \times \vec{p})}{4m^2c^2} \qquad (1\text{-}2)$$

They constructed the nearest-neighbor tight-binding Hamiltonian

$$H_0 = \sum_{\vec{R},\vec{\sigma},i} [|a,i,\sigma,\vec{R}\rangle E_{i,a}\langle a,i,\sigma,\vec{R}| + |c,i,\sigma,\vec{R}+\vec{d}\rangle E_{i,c}\langle c,i,\sigma,\vec{R}+\vec{d}|] + \sum_{\vec{R},\vec{R}',\sigma,i,j} [|a,i,\sigma,\vec{R}\rangle V_{i,j}\langle c,j,\sigma,\vec{R}'+\vec{d}| + \text{h.c.}] + H'_{so} \qquad (1\text{-}3)$$

where h.c. means Hermitian conjugate, $\vec{R}$ are the rock salt lattice positions of the anion, i and j are the basis orbitals for the anion and cation, respectively, σ is the spin (up or down), a and c refer to the anion and cation, respectively, and $\vec{d}$ is the position of the cation relative to the anion in the $\vec{R}$th cell; $\vec{d} = (a_L/2)(1,0,0)$. The spin−orbit part, H'_{so} was expressed as

$$H'_{so} = \sum_{\vec{R},\sigma,\sigma' i} [|c,i,\sigma,\vec{R}+\vec{d}\rangle\lambda_c\vec{L}_c\cdot\vec{\sigma}_c\langle c,i,\sigma',\vec{R}+\vec{d}|] + \sum_{\vec{R},\sigma,\sigma' j} [|a,j,\sigma,\vec{R}\rangle\lambda_a\vec{L}_a\cdot\vec{\sigma}_a\langle a,j,\sigma',\vec{R}|] \qquad (1\text{-}4)$$

Lent et al. used nine orbitals per atom in their basis, each with spin up and down: s, p_x, p_y, p_z, $d_{x^2-y^2}$, $d_{3z^2-r^2}$, d_{xy}, d_{yz}, and d_{xz}. They had to include all five d orbitals because of the importance of the d bands near the bottom of the conduction band, at the X point of the Brillouin zone.

Lent et al.[13] obtained the matrix elements of the tight-binding Hamiltonian by fitting the eigenvalues of the matrix to the energy bands published by Herman et al.[14] They used analytical expressions for the eigenvalues at high-symmetry points to make an initial guess for the parameters. A least-squares fit of the parameters to the calculated energy bands was then performed. The parameters used for PbS are listed in Table 1 (note the large values of the spin−orbit coupling terms). It is quite remarkable that the apparently complicated energy bands of these semiconductors could be reproduced by a simple nearest-neighbor tight-binding Hamiltonian. Once the matrix elements are obtained by fitting the bulk band structure, they can be used for other systems: for example, these authors used their semiempirical matrix elements for PbTe, SnTe, and GeTe to predict the band gaps of $Pb_{1-x}Sn_xTe$, $Sn_{1-y}Ge_yTe$, and $Ge_{1-z}Pb_zTe$ alloys, as functions of compositions x, y, and z. The tight-binding parameterization of the IV−VI energy bands was found to be adequate for reproducing chemical trends, including the Dimmock band reversal phenomenon in $Pb_{1-x}Sn_xTe$.

TABLE 1: Tight-Binding Parameters for PbS (Lent et al.[13])

parameter	value, eV	parameter	value, eV
$E_{s,c}$	−6.546	$V_{p,s}$	0.186
$E_{s,a}$	−13.827	$V_{p,p}$	2.073
$E_{p,c}$	3.486	$V_{p,p\tau}$	−0.281
$E_{p,a}$	−1.153	$V_{p,d}$	−1.142
$E_{d,c}$	9.27	$V_{p,d\tau}$	1.16
$E_{d,a}$	10.38	$V_{d,p}$	−1.54
λ_c	1.559	$V_{d,p\tau}$	0.517
λ_a	−0.211	$V_{d,d}$	−1.67
$V_{s,s}$	−0.364	$V_{d,d\delta}$	0.659
$V_{s,p}$	0.936		

We have used the matrix elements of Lent et al.[13] to study PbS nanocrystallites as a function of size. The following section contains details of the method used to calculate the energy levels and the wave functions. This is followed by a discussion of the results of the calculations.

2. Method of Calculation

In the tight-binding method, the energy levels and wave functions are, respectively, the eigenvalues and the eigenvectors of the Hamiltonian matrix **H**. For lead sulfide, the matrix is composed of 18 × 18 block matrices, describing the interaction between orbitals on the same atom or between orbitals on an atom and on its nearest neighbor. For a lead sulfide cluster containing N atoms, the Hamiltonian is a $18N \times 18N$ matrix. For a spherical crystallite with a diameter of 35 Å, $N = 912$, and we have to diagonalize a 16 416 × 16 416 matrix. Inclusion of spin−orbit coupling introduces complex numbers in the matrix. Diagonalization of such large, complex, Hermitian matrices is both time and memory intensive and is a challenging numerical problem.

The computations were carried out on a Silicon Graphics Indigo 2 workstation. Direct diagonalization was used for clusters containing up to 160 atoms. All of the eigenvalues and eigenvectors were computed for these clusters. In order to store all the matrix elements, a 300-Mbyte partition on the hard disk was used as swap space. Swapping to disk increased the time required for the computations considerably.

Some of the C++ codes for calculations on CdS nanocrystals written by Joffre (M. Joffre and R. Silbey, to be published) were modified and used for the PbS calculations. One of the programs builds a PbS nanocrystallite of the desired size and shape and creates an output file containing the coordinates of each atom, its atomic number, and the number of nearest neighbors for each atom. Another program generates the corresponding hamiltonian matrix and computes its eigenvalues and eigenvectors, using the subroutine ZHEEV from the matrix library LAPACK (which can be obtained from the netlib ftp site). Subroutine ZHEEV calls subroutine ZHETRD, which reduces the complex Hermitian Hamiltonian matrix to the real symmetric tridiagonal matrix **T** by a unitary transformation. Subroutine ZSTEQR then computes all the eigenvalues, and the eigenvectors of **T** using the implicit QL or QR method.

This method worked well for clusters containing up to 160 atoms but started running into time and memory problems above that matrix size. A different method was therefore required for larger clusters. The problem with direct diagonalization is that it did not utilize the special features of the Hamiltonian matrix **H**. Since the matrix is large but contained mostly zeroes, a sparse matrix algorithm was required to compute the eigenvalues and selected eigenvectors of the larger matrices.

Lanczos recursion[15] was used for the larger matrices. The Fortran source code obtained from the Lanczos library at the

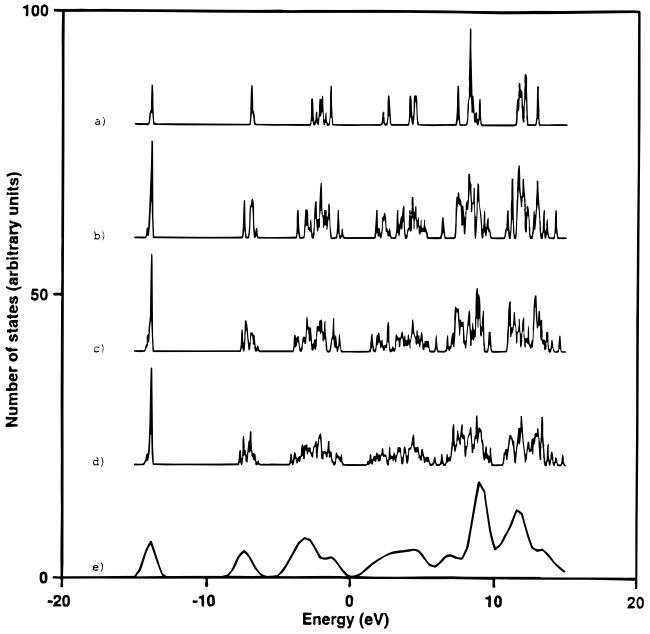

Figure 1. Calculated densities of states ($T = 4.2$ K) for (a) 8-atom PbS cluster, (b) 32-atom PbS cluster, (c) 56-atom PbS cluster, (d) 88-atom PbS cluster, and (e) bulk PbS, broadened with Gaussians ($\sigma = 0.5$ eV).

netlib ftp site was written by Cullum and Willoughby[16] and uses Lanczos tridiagonalization. Lanczos vectors are generated from the complex starting vector $\mathbf{v}_1$ using the following recursion ($i = 1, ..., m$):

$$\beta_{i+1}\mathbf{v}_{i+1} = \mathbf{A}\mathbf{v}_i - \alpha_i\mathbf{v}_i - \beta_i\mathbf{v}_{i-1} \qquad (2\text{-}1)$$

where

$$\alpha_i \equiv \mathbf{v}_i^{\mathrm{H}}\mathbf{A}\mathbf{v}_i \quad \text{and} \quad \beta_{i+1} = ||\mathbf{A}\mathbf{v}_i - \alpha_i\mathbf{v}_i - \beta_i\mathbf{v}_{i-1}|| \qquad (2\text{-}2)$$

and **A** is the Hermitian matrix whose eigenvalues and eigenvectors need to be computed. Each Lanczos matrix generated by this recursive procedure is a real symmetric tridiagonal matrix **T**. Its diagonal entries α_i are the Rayleigh quotients of the matrix **A**. The off-diagonal elements β_{i+1} are real by construction. The Lanczos method involves application of the Rayleigh−Ritz procedure on the sequence of Krylov subspaces. The eigenvalues of **T** are approximations to the eigenvalues of **A**. The main advantage of the Lanczos method is that storage of all the matrix elements is not required. One only needs a subroutine that computes the product **Ax**, where **A** is the user-specified matrix and **x** is any vector.

The Lanczos library program HLEVAL is the main program for the eigenvalue computations. It calls subroutine BISEC to compute eigenvalues of the tridiagonal matrix **T** on user-specified intervals. BISEC uses the bisection method and makes use of the Sturm sequencing property of real symmetric matrices. BISEC computes the **T** eigenvalues with their multiplicities and sorts the computed eigenvalues into two classes: the "good" eigenvalues are accepted as approximations to eigenvalues of the matrix **A**, and the "spurious" eigenvalues, which occur because of the effect of finite precision arithmetic, are rejected. The accuracy of the good **T** eigenvalues as eigenvalues of **A** is then estimated by inverse iteration, using the subroutine INVERR. Once accurate eigenvalues have been obtained, the main program HLEVEC can be used to obtain desired eigenvectors.

These programs were used to obtain the eigenvalues and eigenvectors of the Hamiltonian H. For PbS clusters containing 160 atoms and clusters of smaller sizes, all the eigenvalues were obtained and were identical to the eigenvalues obtained by direct diagonalization using the LAPACK library subroutine ZHEEV. For larger matrices, the starting vector was chosen to have a large projection on states near the gap. The eigenvalues were determined in a small region around the gap. The eigenvectors for the HOMO and LUMO states were determined using program HLEVEC.

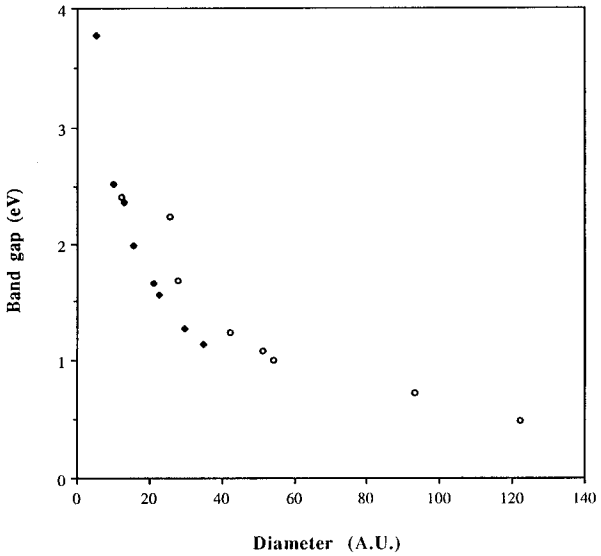

Figure 2. Band gap for PbS clusters. Black diamonds represent the temperature-adjusted calculations. Circles represent the experimental data of Wang et al.[9]

TABLE 2: Calculated Band Gaps for Spherical PbS Nanoclusters

no. of atoms	diameter, Å	band gap (eV) w/o temp adjustment
8	5.2	3.654
32	9.9	2.393
56	12.9	2.240
88	15.4	1.862
160	19.5	1.552
208	21.2	1.538
280	22.8	1.439
552	29.5	1.145
912	35.0	1.015

3. Energy States of the Nanocrystallites

The PbS crystals considered in this work were spherical and stoichiometric. The origin was chosen to lie between an anion and a cation. Since all of the eigenvalues were computed for the smaller crystallites, the densities of states were calculated. Figure 1 compares the densities of states for spherical PbS crystals with that for bulk PbS. The density of states for the bulk PbS crystal was obtained by sampling the Brillouin zone and diagonalizing the 36×36 Hamiltonian for each chosen wave vector **k**. It is evident from the figure that as the number of atoms in a cluster increases, the gaps begin to fill in, and the density of states smoothly approaches the bulk density of states.

For nanoclusters, the band gap is defined to be the difference between the energies of the HOMO and LUMO states. Table 2 shows the calculated band gaps for spherical stoichiometric PbS nanoclusters; Figure 2 compares the calculated band gap for the spherical PbS nanoclusters with the experimental results of Wang et al.[10] The measurements were made at room temperature, whereas the calculations for PbS are based on the band gap of 0.286 eV measured at 4.2 K.[17] The band gap for bulk PbS increases with temperature to a value of 0.410 eV at 300 K.[10] If we assume that the variation of the gap with

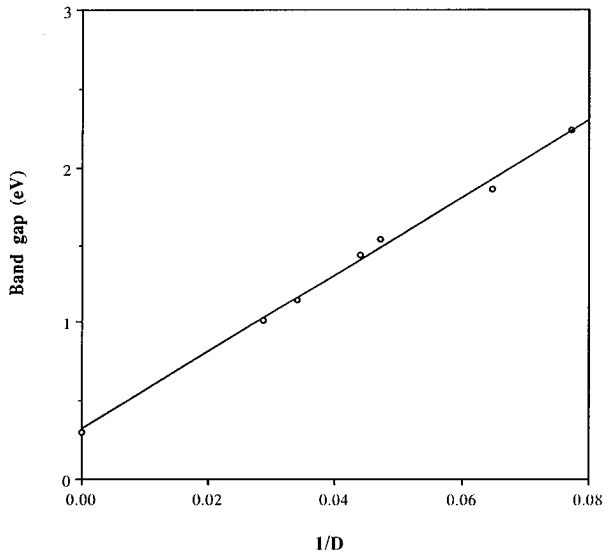

Figure 3. Dependence of the calculated band gap ($T = 4.2$ K) on the diameter for spherical PbS clusters. The line represents a linear fit to the data: Band gap $= 0.311 + 24.89/D$; $R^2 = 0.996$.

temperature is the same for the clusters as for the bulk crystal, then this difference of 0.124 eV needs to be added to the calculated values of the band gap. These temperature-adjusted calculated values are shown in Figure 2. The agreement with experimental data is quite good, given that the experimental values are obtained from samples with a large cluster size distribution. For instance, for a 50-Å PbS sample, the largest deviation in size was $<\pm 50\%$, with the average deviation being $<\pm 20\%$.

It was interesting to determine the dependence of the calculated band gap on the crystal diameter D. Figure 3 shows that the calculated band gap for spherical PbS nanoclusters varies linearly with $1/D$. The crystal diameter can be related to the wave vector **k** using the particle in a sphere picture. The allowed **k** for a spherical cluster is then $2\pi/D$. Since the band gap occurs away from the center, at the L-point of the Brillouin zone for bulk PbS, the allowed **k** would lie at a distance of $2\pi/D$ from the L point of the Brillouin zone. Figure 3 implies that the band gap is linear in **k**. This is different from the parabolic dependence predicted by effective-mass theory. To explain this result, the variation of the band gap with the wave vector **k** for bulk PbS was examined for small deviations from the L point. The band gap for bulk PbS was also found to be linear in **k** near the L point, which explained the observed $1/D$ dependence of the band gap for the clusters. Of course, very close to $\mathbf{k} = 0$, the band gap should be proportional to $1/D^2$. However, because of the small bulk band gap and the small effective mass, the dependence becomes linear in **k** at finite values of **k**.

The band gap of a nanocrystal determines the frequency above which it absorbs light. The tight-binding theory can also be used to predict the shape of the absorption spectrum. If it is assumed that all electronic transitions have the same transition moments, the absorption spectrum will be equal to the joint density of states, which is plotted for spherical clusters containing 32, 56, 88, and 160 atoms in Figure 4. The figure demonstrates that the absorption moves into the visible range as the number of atoms in the cluster increases. The predictions of the theory should be tested by comparing the predicted absorption spectra to the UV−vis spectra for monodisperse PbS nanoclusters.

4. Analysis of the Eigenvectors

Analysis of the eigenvectors provides additional information about the gap states. Table 3 contains information about the

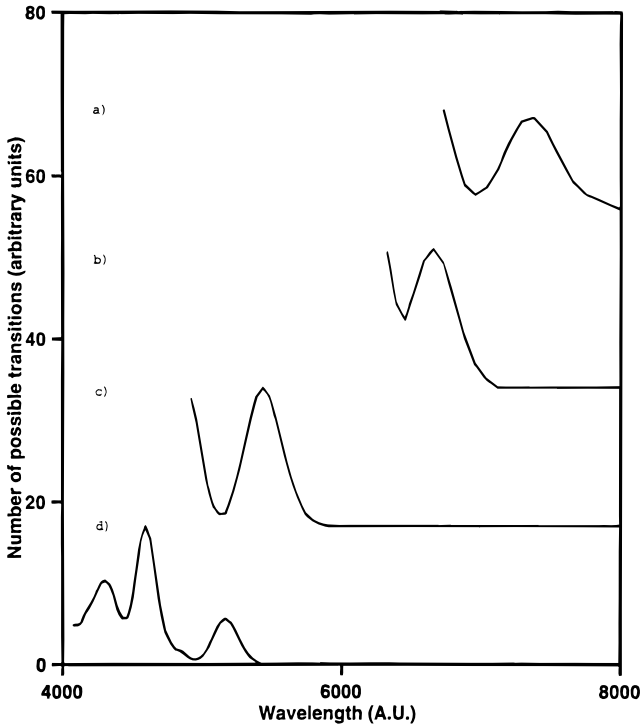

Figure 4. Calculated joint density of states ($T = 4.2$ K) for spherical PbS clusters with (a) 160 atoms, (b) 88 atoms, (c) 56 atoms, and (d) 32 atoms, broadened with Gaussians ($\sigma = 0.06$ eV).

TABLE 3: Character of the HOMO and LUMO States of PbS

no. of atoms	diameter, Å	Ss	Sp	Sd	Pbs	Pbp	Pbd
			HOMO				
8	5.15	0	0.76	0.01	0.08	0.15	0.01
32	9.85	0	0.79	0.01	0.13	0.06	0.02
56	12.94	0	0.76	0.01	0.13	0.08	0.03
88	15.43	0	0.76	0.01	0.14	0.07	0.03
208	21.20	0	0.74	0.01	0.15	0.07	0.03
280	22.80	0	0.74	0.01	0.16	0.07	0.03
552	29.54	0	0.73	0.01	0.16	0.07	0.03
912	35.00	0	0.72	0.01	0.16	0.07	0.03
bulk PbS		0	0.77	0	0.19	0	0.03
			LUMO				
8	5.15	0	0.17	0.04	0	0.78	0
32	9.85	0	0.16	0.09	0	0.73	0.02
56	12.94	0	0.14	0.1	0	0.74	0.01
88	15.43	0	0.13	0.1	0	0.76	0.01
208	21.20	0	0.13	0.12	0.01	0.73	0.01
280	22.80	0	0.13	0.12	0.01	0.73	0.01
552	29.54	0	0.12	0.12	0.01	0.74	0.01
912	35.00	0	0.11	0.12	0.01	0.74	0.01
bulk PbS		0	0	0.15	0	0.85	0

HOMO and LUMO eigenstates for the spherical PbS clusters. In the table, Ss, Sp, Sd, Pbs, Pbp, and Pbd refer to the probability of being in sulfur s, sulfur p, sulfur d, lead s, lead p, and lead d states, respectively. The values for the clusters are compared to the corresponding values for the bulk PbS crystal. As the size of the crystal increases, these values approach the bulk values. The bulk HOMO state is mainly composed of the p state of sulfur; the bulk LUMO state is mainly composed of the p state of lead, in agreement with chemical intuition. The molecule of PbS can be considered to be formed by transferring the two 6p electrons of lead to the 3p orbitals of sulfur. In that case, the lowest excited state would mainly consist of the 6p state of lead.

Finally, analysis of the eigenvectors provides information about the surface character of the HOMO and LUMO states.

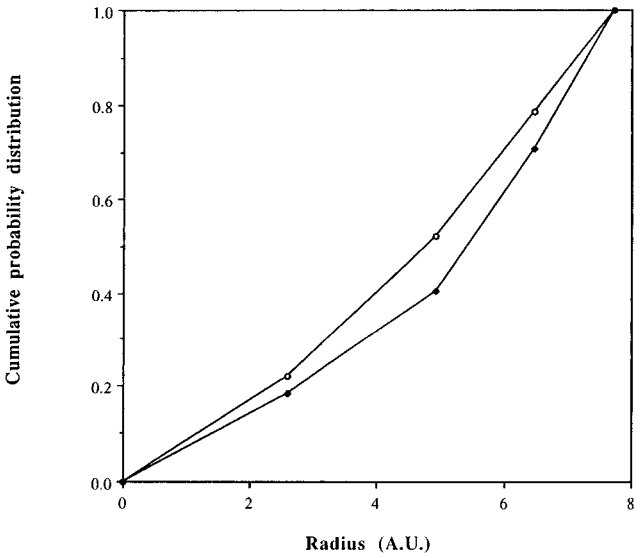

Figure 5. Probability distribution for the gap states of an 88-atom spherical PbS cluster. Circles represent values for the HOMO state, and black diamonds represent values for the LUMO state.

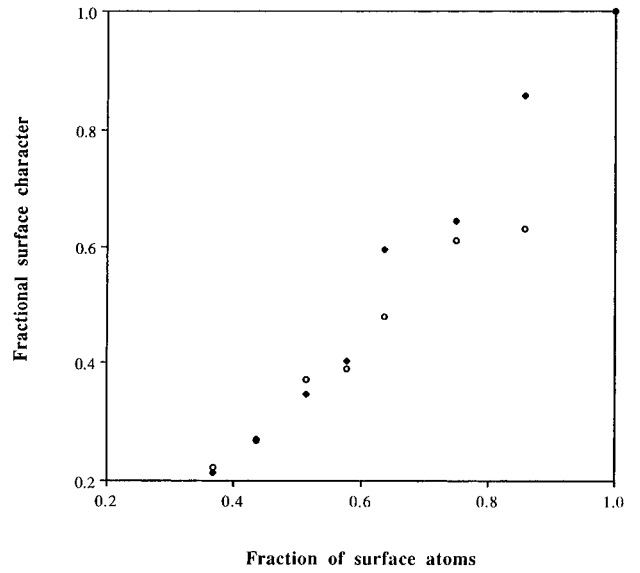

Figure 6. Surface character of the gap states of spherical PbS clusters. Circles represent values for the HOMO states, and black diamonds represent values for the LUMO states.

Figure 5 plots the cumulative probability distribution (the probability of an electron being in an orbital located on an atom within the radius R) vs R for the HOMO and LUMO states of a spherical PbS cluster containing 88 atoms. The plot is similar to those for the PbS clusters of other sizes and shows that eigenfunctions corresponding to the HOMO and LUMO states extend throughout the cluster. This conclusion is reinforced by Figure 6, in which the fraction of surface character is plotted vs the fraction of surface atoms for the HOMO and LUMO states of spherical PbS nanocrystallites. The plots indicate that the orbitals localized on surface atoms do not dominate the HOMO and LUMO states. Since the HOMO and LUMO states are delocalized throughout the cluster, electron and hole recombination should be facile in PbS nanoclusters, and the lifetime of the excited state should therefore be short. This prediction can be tested by fluorescence lifetime measurements for PbS nanoclusters.

Similar delocalized gap states were obtained by Nair et al.[5] from their tight-binding calculations for GaAs quantum dots. We have not (like Nair et al.[5] and unlike Lippens and Lannoo[2,3]) removed any dangling orbitals from the basis. As Nair et al. point out, their result is in agreement with the calculations of Bachelet et al.[18] For a cluster with a simple cubic lattice, using a tight-binding model with uncoupled s−p orbitals and nearest-neighbor interaction, Bachelet et al. found that surface states were present only when the on-site energies of the surface atoms and interior atoms differed by an amount greater than the nearest-neighbor off-diagonal matrix element. Therefore, in this case as well, the absence of surface states is due to the fact that equal on-site energies have been chosen for all chemically similar atoms. These on-site energies could be modified for surface atoms to test the importance of surface effects.

5. Conclusions

We have demonstrated that the tight-binding method predicts the size dependence of the band gap for PbS nanoclusters in reasonable agreement with experimental data. The densities of states for the nanoclusters approach the bulk density of states with increasing cluster size. The s, p, and d character of the HOMO and LUMO eigenstates also approaches that for the bulk eigenstates as the cluster size increases. In PbS, surface states do not dominate the HOMO and LUMO eigenstates, which are spread throughout the cluster. Delocalized HOMO and LUMO states should result in rapid electron−hole recombination and short excited state lifetimes in PbS nanoclusters. The small surface character of the gap states is a related to the assumption of equal on-site energies for surface and bulk atoms. This assumption could be modified to incorporate the effect of interaction of the surface atoms with other atoms.

Acknowledgment. R.S.K. thanks Prof. Robert Brown for very useful discussions regarding the Lanczos method. Manuel Joffre wrote the C++ codes for CdS nanoclusters (which were modified and used for PbS), during his postdoctoral work at MIT. R.S.K. also thanks the NSF for his graduate fellowship. This research was supported by NSF under Grant No. CHE-9312413.

References and Notes

(1) Henglein, A. *Chem. Rev.* **1989**, *89*, 1861.
(2) Lippens, P. E.; Lannoo, M. *Phys. Rev. B* **1989**, *39*, 935.
(3) Lippens, P. E.; Lannoo, M. *Phys. Rev. B* **1990**, *41*, 6079.
(4) Rama Krishna, M. V.; Friesner, R. A. *J. Chem. Phys.* **1991**, *95*, 8309.
(5) Nair, S. V.; Ramaniah, L. M.; Rustagi, K. C. *Phys. Rev. B* **1992**, *45*, 5969.
(6) Hill, N. A.; Whaley, K. B. *J. Chem. Phys.* **1993**, *99*, 3707.
(7) Ekimov, A. I.; Onushchenko, A. A. *JETP Lett.* **1981**, *34*, 345.
(8) Efros, A. I. L.; Efros, A. L. *Sov. Phys. Semicond.* **1982**, *16*, 772.
(9) Brus, L. E. *J. Chem. Phys.* **1984**, *80*, 4403.
(10) Wang, Y.; Suna, A.; Mahler, W.; Kasowski, R. *J. Chem. Phys.* **1987**, *87*, 7315.
(11) Vogl, P.; Hjalmarson, H. P.; Dow, J. D. *J. Phys. Chem. Solids* **1983**, *44*, 365.
(12) Wang, Y. *Acc. Chem. Res.* **1991**, *24*, 133.
(13) Lent, C. S.; Bowen, M. A.; Dow, J. D.; Allgaier, R. S.; Sankey, O. F.; Ho, E. S. *Superlattices Microstruct.* **1986**, *2*, 491.
(14) Herman, F.; Kortum, R. L.; Ortenburger, I. B.; Van Dyke, J. P. *J. Physiq.* **1968**, *29* (Suppl. C4), 62.
(15) Lanczos, C. *J. Res. Natl. Bur. Stand., Sect. B* **1950**, *45*, 225.
(16) Cullum, J. K.; Willoughby, R. A. *Lanczos Algorithms for Large Symmetric Eigenvalue Computations;* Birkhauser: Boston, 1985; Vols 1 and 2.
(17) Mitchell, D. L.; Palik, E. D.; Zemel, J. N. *Proc. 7th Int. Conf. Phys. Semicond.* **1964**, 325.
(18) Bachelet, G. B.; Bassani, F.; Bourg, M.; Julg, A. *J. Phys. Chem.* **1983**, *16*, 4305.
(19) Ren, S. Y.; Dow, J. D. *Phys. Rev. B* **1992**, *45*, 6492.

JP952869N